

Feedback topology and XOR-dynamics in Boolean networks with varying input structure

L. Ciandrini,^{1,*} C. Maffi,^{2,†} A. Motta,³ B. Bassetti,^{3,4} and M. Cosentino Lagomarsino^{3,4,‡}

¹*Università di Pavia, Dip. di Fisica Nucleare e Teorica, Via Bassi 6, 27100 Pavia, Italy*

²*Laboratoire de Biophysique Statistique, EPFL SB ITP, CH-1015, Lausanne, Switzerland*

³*Università degli Studi di Milano, Dip. Fisica, Via Celoria 16, 20133 Milano, Italy*

⁴*I.N.F.N. Milano, Italy*

(Dated: September 9, 2008)

We analyse a model of fixed in-degree Random Boolean Networks in which the fraction of input-receiving nodes is controlled by a parameter γ . We investigate analytically and numerically the dynamics of graphs under a parallel XOR updating scheme. This scheme is interesting because it is accessible analytically and its phenomenology is at the same time under control, and as rich as the one of general Boolean networks. Biologically, it is justified on abstract grounds by the fact that all existing interactions play a dynamical role. We give analytical formulas for the dynamics on general graphs, showing that with a XOR-type evolution rule, dynamic features are direct consequences of the topological feedback structure, in analogy with the role of relevant components in Kauffman networks. Considering graphs with fixed in-degree, we characterize analytically and numerically the feedback regions using graph decimation algorithms (Leaf Removal). With varying γ , this graph ensemble shows a phase transition that separates a tree-like graph region from one in which feedback components emerge. Networks near the transition point have feedback components made of disjoint loops, in which each node has exactly one incoming and one outgoing link. Using this fact we provide analytical estimates of the maximum period starting from topological considerations.

PACS numbers: 89.75.Hc, 05.65.+b, 89.75.Fb

I. INTRODUCTION

Biological networks are graphs representing the basic interactions between molecules in a living cell [1, 2, 3, 4]. They are generally composed of a fairly large number of elements and for this reason it is unfeasible to treat all the biochemical processes in detail. For example, a transcription network [5, 6, 7] of a simple cell counts some thousands of nodes, which represent the genes of a cell. Given the interaction structure, it is important to establish which genes are active in a given time or environment, or under a given stimulus. In order to fulfill this task, it is necessary to develop coarse-grained models for gene expression, such as discrete systems, in which variables on the nodes represent the (discretized) expression of single genes, and directed connections stand for their interactions [8, 9]. These abstract models are useful to study on general grounds the emergent cooperative behaviour of gene expression, as biological function is increasingly being recognized as emerging from global phenomena rather than from the expression of single genes [1, 10, 11].

The simplest model of this kind are Random Boolean Networks (RBNs) introduced by S. Kauffman in 1969 [12]. In this model, N elements take binary values and interact with some random coupling functions. In the

standard Kauffman model, the configuration of an element is set by Boolean functions whose values depend on a fixed number k of inputs. The system is specified by its topology (a graph with k inputs regulating each node), a synchronous updating scheme and the choice for the ensemble of Boolean functions (for an introductory review see Refs. [13, 14, 15]). Technically speaking, the behaviour of the system is fully characterized by its cycles (or fixed points) and their basins of attraction. If a cycle contains exponentially many (in N) configurations, the behaviour is called chaotic. Otherwise it is called ordered. According to the original Kauffman interpretation, if the system is in a chaotic state, it cannot exhibit specific behaviour in response to external stimuli. More specifically, a realization of the model is interpreted as a genome and an attractor as a possible cell type. If the corresponding cycle period is too long, this hypothetical cell type would never realize it. For this reason, networks of biological interest should lie between the ordered and the chaotic phase (the so-called critical networks [16]), where attractor cycles are neither too short nor exponential.

There are two problems concerning Kauffman's model in relation with genetic networks. First, the ensemble contains only graphs entirely made of feedback, while typically this is not the case of biological (e.g. transcription) networks, which usually have some "sensor" nodes that respond to external conditions [17, 18, 19]. Thus, it is useful to modify the model and consider networks with well-defined input structure. The second problem is connected to the choice of the ensemble of Boolean functions. While on biological grounds it is difficult to characterize

*Electronic address: Luca.Ciandrini@pv.infn.it

†Electronic address: carlo.maffi@epfl.ch

‡Electronic address: Marco.Cosentino-Lagomarsino@unimi.it

this class, from a mathematical viewpoint the choice of functions strongly conditions the behaviour of the model. Indeed, since most functions are constant, or “canalizing” [14, 15] with respect to some variables, this creates an “effective topology”, which does not correspond to the underlying interaction graph. For this reason, the study of attractors in Kauffman networks is complex (for recent results see, for example, [20, 21, 22]). Also the study of critical networks with canalizing Boolean functions leads to the conclusion that this choice does not decrease attractor sizes and render the model more well-behaved as previously expected [20].

In this work, we address these questions in a controlled way, with the following choices. First, we work with a graph ensemble with a parameter that regulates the fraction of input nodes, following the approach of Refs. [23, 24, 25, 26]. Secondly, we choose to use the ensemble of XOR or totally non-canalizing functions. This simplified choice strictly relates the dynamics with the topology. In other words, the output changes if any one of the inputs changes its value. Roughly speaking, on biological grounds, one expects that in a regulatory network the role of constant functions should be marginal, because the interactions are conserved by selective pressure only if they are useful. From the technical viewpoint, this dynamics has the advantage to be approachable with linear algebra using the finite Galois field $GF(2)$ [27, 28], the set $\{0, 1\}$ where addition between elements is equivalent to the logic XOR and multiplication to the logic AND.

Our main results are the following. With varying γ , we observe a phase transition, similar to the one observed in Kauffman networks, from a region characterized by an ordered dynamic behaviour to a region in which the dynamics is chaotic. From a topological point of view the same transition divides a region characterized by tree-like graphs from one in which extensive feedback is present. The structure of networks around the critical point appears simplified, in the sense that the feedback regions of this kind of networks are organized in simple disjoint loops. We use the topological structure of critical point networks to estimate the maximum period times. The paper is organized as follows. After giving the basic definitions in Section II, we present the main results in Section III. In the last sections we discuss the results.

II. DEFINITION OF THE MODEL

We consider networks of N nodes, of which only M receive input, and define $\gamma = M/N$. Each of these regulated nodes receives inputs from exactly k randomly and independently chosen other nodes. Consequently the in-degree is k or 0, while the out-degree distribution is binomial, and in the “thermodynamic” limit $N \rightarrow \infty$ and γ constant is well approximated by a Poisson distribution of mean $k\gamma$,

$$p_{out}(\gamma k, n) = e^{-\gamma k} \frac{(\gamma k)^n}{n!}.$$

As a consequence, the graphs contain nodes with no output (*leaves*) and $N - M$ *roots*, i.e. variables without inputs (Fig. 1). This ensemble is conventionally used in diluted spin-glass models and constraint-satisfaction networks [29, 30]. The standard Kauffman graph ensemble can be obtained considering the special case $\gamma = 1$ in which all variables are regulated. The graph ensemble is

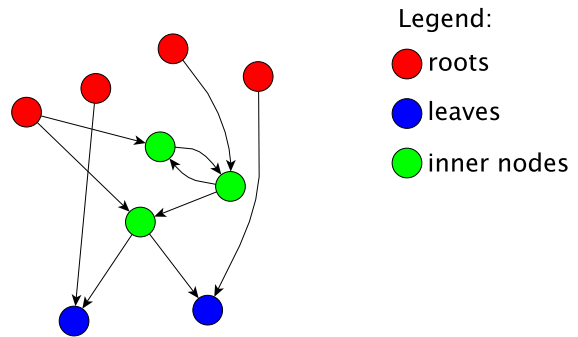


FIG. 1: A network with $N = 9$, in-degree $k = 2$ and $\gamma \simeq 0.55$. Red circles (colors online) indicate roots, blue circles leaves and green circles the inner nodes.

specified by a $M \times N$ connectivity matrix A where $a_{ij} = 1$ if the edge $j \rightarrow i$ exists, and zero otherwise. It is useful to arrange the columns of A in order to reserve the first M indices to the nodes that receive inputs. This matrix can further be divided into two submatrices $A = (S \mid R)$. S is the $M \times M$ matrix that describes the interaction between regulated elements, while the columns of R contain the information on the outputs of the free variables.

We consider a dynamics on the graphs of this ensemble, specified by assigning Boolean variables to each of the N nodes and interactions through XOR coupling functions. A global state $\vec{\sigma}$ is defined as the set of configurations assumed by all the nodes of the network. The configuration space, formed by all global states, contains 2^N states. Since the system is finite, starting from some initial global state, the deterministic dynamics leads to periodically repeated states, possibly after a transient time. In other words, the system performs a trajectory in the state space and eventually arrives to an *attractor* of length T , where the states are periodic in time. The attractor has length T if $\vec{\sigma}(t+T) = \vec{\sigma}(t)$. We call this a T -cycle or a *fixed point*, in case of unitary length. The *basin* of attraction of an attractor is the set of global states that reach the attractor, including the attractor states. A *transient state* is a state that belongs to a basin but is not part of an attractor. The N -dimensional Boolean vector $\vec{\sigma}(t)$ can be written as $\vec{\sigma}(t) = (\vec{x}(t), \vec{y}(t))$. The M -dimensional vector $\vec{x}(t)$ denotes the state of the regulated variables and the $(N - M)$ -dimensional vector $\vec{y}(t)$ the (constant) state of the root variables ($\vec{y}(t) = \vec{y}(0) = \vec{y}$).

The synchronous update at time t is determined by random XOR functions, or, equivalently, by the linear op-

eration in the Galois field $GF(2)$ [26, 27]

$$\vec{x}(t+1) = A\vec{\sigma}(t) + \vec{b} = S\vec{x}(t) + R\vec{y} + \vec{b}, \quad (1)$$

where \vec{b} is a random M -dimensional Boolean vector containing the information relative to the nature of regulating functions. The components b_i of \vec{b} are 0 or 1 with probability $\frac{1}{2}$. The evolved state after t steps is

$$\vec{x}(t) = S^t \vec{x}(0) + \sum_{i=0}^{t-1} S^i (R\vec{y} + \vec{b}) = S^t \vec{x}(0) + \Sigma(t)(R\vec{y} + \vec{b}), \quad (2)$$

where $\Sigma(t) \doteq \sum_{i=0}^{t-1} S^i$ (the symbol \doteq stands for a definition). One can observe from Eq. (2) that the dynamics is controlled by the topology through the interaction matrix. The peculiarity of the XOR dynamics is that every change of one (or an odd number of) input in a function determines a change in the output. We shall demonstrate that feedback components of the graph are the only relevant region needed for characterizing the dynamic behaviour of the whole network.

III. RESULTS

A. General features of XOR-dynamics

The discrete XOR dynamics defined above allows to derive some simple general properties that will be used in the following.

Firstly, linearity implies that the cycles have a least common multiple (LCM) structure, where longer nontrivial cycles can be constructed by combining smaller ones. As a consequence, if a network shows a set $\{T_i\}$ of cycle lengths, then a cycle of length $T' = \text{lcm}\{T_i\}$ also exists.

From Eq. (2) a global state $\vec{\sigma}(t)$ belongs to a T -cycle if $\vec{\sigma}(T+t) = \vec{\sigma}(t)$, which gives the condition

$$\left[(1 + S)\vec{x}(0) + R\vec{y} + \vec{b} \right] \in \ker \Sigma(T),$$

i.e. the vector on the left hand side is sent to $\vec{0}$ by the function Σ for some T . In the eventuality of $T = 1$ the same condition becomes

$$(1 + S)\vec{x}(0) = R\vec{y} + \vec{b}.$$

The fact that the dynamics can only have transients or cycles translates into the formula

$$S^{l+t_m} = S^l, \quad (3)$$

where l is the smallest integer such as $\ker S^l = \ker S^{l+1}$ (the length of the longest transient) and t_m is the maximum cycle length (without repetitions) for the map $\vec{x} \rightarrow S\vec{x}$. This quantity can be related to the maximum cycle for the complete dynamics using the fact that $\Sigma(2t_m + l) = \Sigma(l)$, so that for any given initial condition,

$$\vec{x}(2t_m + l) = S^l \vec{x} + \Sigma(l)(R\vec{y} + \vec{b}) = \vec{x}(l),$$

which implies that the maximum cycle for the full dynamics is at most $T_{max} = 2t_m$.

We now give a heuristic argument connecting the algebraic properties of S with statistical properties of the dynamics. If $m(T)$ is the multiplicity of T -cycles, and $\mathcal{B}(T)$ is the number of configurations in the basin of attraction of each T -cycle, one must have

$$2^N = \sum_T \mathcal{B}(T)m(T).$$

The elements belonging to a basin of attraction are built adding $\vec{z} \in \ker S^l$ to a fixed system state \vec{x} of a T -cycle (Note that also elements $\vec{z} = \vec{0}$ are taken in consideration and thus \vec{x} itself is considered part of the basin). Thus, each attractor of length T has a basin of attraction whose dimension is $\mathcal{B}(T) = T\mathcal{B}(1) = T2^d$, where $d = \dim(\ker S^l)$. To compute the probability of a cycle one has to provide an estimate for $m(T)$. From previous work [23], we know that generally the average number of fixed points is $m(1) = 2^{N-M}$, this can be also the typical value, depending on the graph ensemble and the value of γ . Since adding a fixed point to the elements of a T -cycle leads to a cycle of the same length, $m(T)$ has a prefactor $m(1)$. Supposing that the contribution of the longer cycles is of order one, one can write, $m(T) \sim m(1)$, or in other words the multiplicity of cycles can be estimated using the number of fixed points. In this hypothesis, the probability $p(T)$ that a state is in the basin of attraction of a T -cycle is

$$p(T) = \frac{1}{2^N} \mathcal{B}(T)m(T) \simeq 2^{d-M} T. \quad (4)$$

Note that this estimate holds only for the values of T that are possible. If T_{max} grows faster than M , $\sum_T T \simeq T_{max}$ implying that $P(T)$ will be concentrated on T_{max} . Equation (4) has a practical implication for simulations: given a realization of a network, it enables to simulate only few initial conditions to find the value of T_{max} that is reached with highest probability. These facts will help understanding some dynamic features of the networks around the critical line.

B. Simulations

We will now turn our attention to direct simulations of the model presented in Section II. In these simulations one has to sample a number of ensemble graphs, and for each graph, a number of random initial conditions. The choice of the average performed and the quantity of interest leads to the definition of different observables.

The simplest observables relate to the fixed points of the dynamics. Figure 2.a shows the probability of finding at least one fixed point as a function of the parameter γ . Fixed points are typically exhibited for low values of γ while they become rare for higher values, with a sharp threshold in between. One can notice that increasing

system size makes more evident the two distinct regimes. Another way of presenting this result is given in Fig. 2.b, which shows the variance of $p(1)$ depending on γ . This plot has a peak whose maximum value shifts with increasing number of nodes. Accurate location of the transition point in Figs. 2.a and 2.b is rendered difficult by the fact that for larger system sizes, where the results should be more reliable, sampling efficiently the initial conditions becomes difficult.

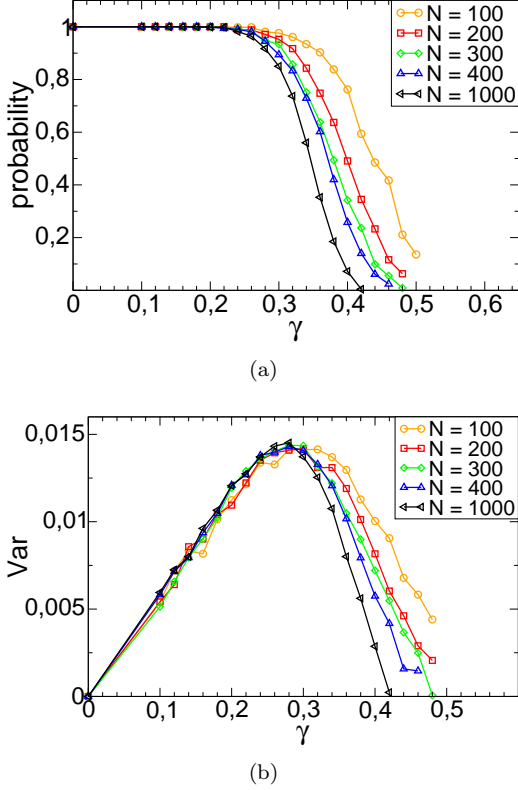


FIG. 2: **Simulations of dynamics: Fixed points.** (a) Probability of finding at least one fixed point for different values of N ($k = 3$). The probability drops down after a certain value of γ . (b) Variance of the probability of observing one fixed point as a function of γ . The plot is obtained by averaging the fraction of 10^3 random initial configurations reaching a fixed point (on a fixed graph) over 10^3 graph realizations at a given γ .

These results show signatures of a dynamical transition point γ_c^d which marks the border between a region with typically fixed points and a region where cycles dominate on fixed points. According to Eq. 4, for $T = 1$, the shape of the curves indicates that d becomes significantly different from M after a certain value of γ . In the large system limit, if $d \ll M$ one expects that $p(1)$ is negligible and the probability of finding at least one fixed point drops to zero. At the transition point the probability of a fixed point and its variance should drop to zero in the thermodynamic limit. The effects of finite size are evident as the measured transition point strongly depends

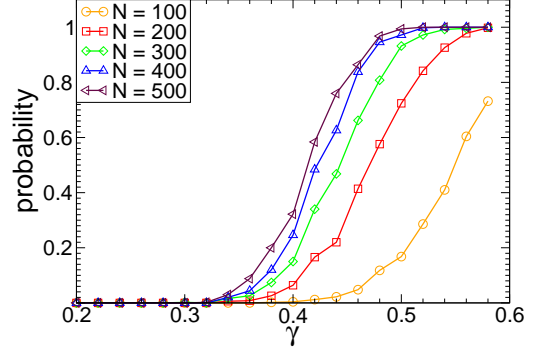


FIG. 3: **Simulations of dynamics: Long cycles.** The plot presents the fraction of periods larger than the cutoff (10^6). At N and γ given, we sampled 10^3 random networks and for each network we evaluated 10 initial conditions.

on the system dimension. We will investigate these effects later (Section III C). Note that the fraction of fixed points just below the threshold decreases unexpectedly with N . However, this has no physical meaning and is connected to the fact that the number of initial conditions is kept constant and consequently larger systems are increasingly under-sampled.

The same transition is visible by quantifying the length of cycles. However this task is computationally hard already for $N \simeq 100$, which strongly limits this kind of simulations. Indeed, to implement these simulations, it is necessary to impose a cutoff on the length of the maximum period observed. Figure 3 shows the fraction of networks with a period larger than the cutoff imposed, given N and γ . This quantity grows rapidly beyond a characteristic parameter value that changes even more with the system dimension, and the transition point is difficult to locate precisely. Hence, it is necessary to find effective methods to investigate the dynamics and this problem will be discussed in Section III E after having studied the feedback topology of graphs in correspondence with the transition.

C. Feedback topology and Leaf Removal algorithms

In this section, we analyze the topology of the graphs. The question that we want to address is whether the dynamic transition is connected to a change in the feedback topology of the underlying graphs.

To study the feedback regions we use three modified versions for directed graphs of the Leaf Removal (LR) decimation algorithm [30, 31]. A graph decimation technique consists in erasing iteratively nodes and links with some specified prescriptions. The variants we implemented remove tree-like parts of the graph, leaving the components with feedback. Network regions not removed by the algorithms are called *feedback core of the graph* or simply *core*. It is possible to study analytically the be-

haviour of the algorithms in the mean-field approximation [32], considering for example the fraction of nodes in the core. The LR algorithms define a dynamics for the probability $p_n(t)$ that a regulated node has n inputs at iteration t , (i.e. of having n ones on a row of the matrix S), and for the probability $f_n(t)$ that a node has n outputs at iteration t (n ones on a column of S). We study LR algorithms analytically with mean-field equations and compare with numerical simulations.

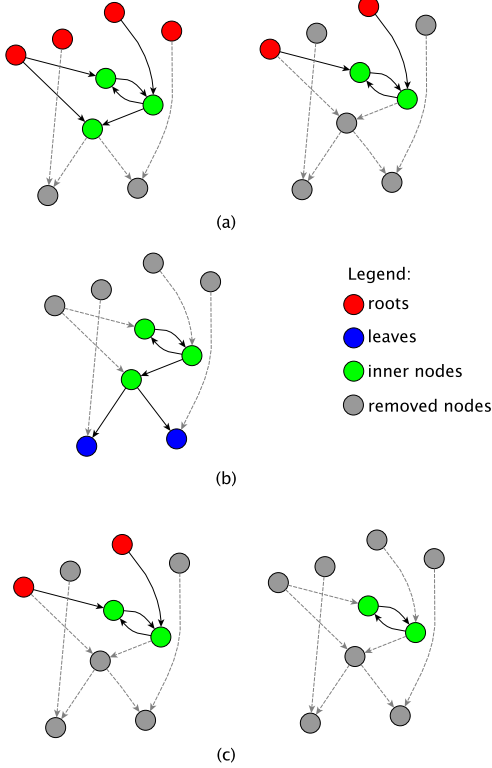


FIG. 4: **Leaf Removal algorithms.** (a) Iterations of LRu for the graph presented in Fig. 1. The LRu removes iteratively the non regulating variables and their links (light grey nodes and dotted arrows). In this case the algorithm stops after two steps. (b) Iterations of LRd. The LRd removes iteratively the regulating variables that are not regulated and the associated links (light grey nodes and dotted arrows). Only one step is possible in this case. (c) Iterations of LRb. First the LRu is applied and then all non-regulating nodes are taken off with the LRd.

The first LR variant we analyze is the so called *Leaf Removal Up* (LRu) [26]. In each step of this algorithm the variables without outgoing links (the leaves) are removed together with its incoming links. The procedure is iterated until each variable has at least one outgoing edge (Fig. 4.a). The solution of the mean-field flux equations for $f_n(t)$ is (see Ref. [26] and Appendix A):

$$\begin{cases} f_0(\bar{t}) = -\bar{t} + e^{-\lambda(\bar{t})} \\ f_n(\bar{t}) = e^{-\lambda(\bar{t})} \frac{\lambda(\bar{t})^n}{n!}, \quad n > 0, \end{cases}$$

where $\bar{t} = t/M$ and $\lambda(\bar{t}) = \gamma k(1 - \bar{t})$. The algorithm

stops at the reduced time \bar{t}_{up}^* and the number M_c^{up} of remaining nodes is

$$M_c^{up} = M z_{up}^*,$$

where $z_{up}^* = 1 - \bar{t}_{up}^*$ is a function of γ and represents the fraction of nodes belonging to the LRu core on the total of regulated nodes. Figure 5.a compares the analytic curve for z_{up}^* as a function of γ with numerical results. Varying γ , there is a singularity which is a signature of a phase transition between a region characterized by graphs entirely removed by the algorithm ($z_{up}^* = 0$) and a region in which the amount of remaining nodes after the process augments when γ is increased. These regimes are separated by the “critical point” $\gamma_c^{up} = k^{-1}$ found with mean field equations.

The second variant we analyze is the *Leaf Removal down* algorithm (LRd) [33], which, in a similar way as above, removes iteratively the nodes with no incoming links, together with their outgoing edges, until there are no more roots (see Fig. 4.b). The mean-field flux equations (shown in Appendix A) for $p_n(t)$ have solution

$$\begin{cases} p_0(z) = (z - 1) + (1 - \gamma z)^k \\ p_n(z) = \binom{k}{n} (\gamma z)^n (1 - \gamma z)^{k-n}, \quad n > 0, \end{cases}$$

where $z = 1 - \bar{t}$. When the algorithm halts the amount of nodes in the LRd core is given by

$$M_c^{down} = M z_{down}^*.$$

The critical value $\gamma_c^{down} = k^{-1}$ divides the networks with a non-vanishing core in the large N limit from the ones that are removed by LRd. The plot of $z_{down}^*(\gamma)$ is presented in Fig. 5.b and compared with simulations.

The last version of LR we consider is the combination of LRu and LRd which we call *Leaf Removal both* (LRb). From the point of view of the dynamics this algorithm first removes all the nodes which do not regulate the *core* and successively it removes the set of nodes that are fixed, at most after a transient time, the initial conditions given. From the topological viewpoint it leaves all and only the nodes involved in feedback cycles (Fig. 4.c). It can be checked that a single iteration of LRu and LRd is sufficient for this. The LRu algorithm stops at a matrix with M_c^{up} rows having k entries and whose remaining rows are empty. When LRd is applied to this matrix, elimination of all empty rows and columns leaves with $M_c^{both} = M_c^{up} z_{down}^* = M z_{down}^* z_{up}^*$ nodes, and the following per-row and per-column probabilities of n entries

$$\begin{cases} p_0 = f_0 = 0 \\ p_n = (z_{down}^*)^{-1} \binom{k}{n} (\gamma z_{down}^*)^n (1 - \gamma z_{down}^*)^{k-n} \\ f_n = (z_{up}^*)^{-1} e^{-\lambda(\bar{t}_{up}^*)} \frac{\lambda(\bar{t}_{up}^*)^n}{n!}. \end{cases} \quad (5)$$

In this case $z_{both}^* \doteq z_{down}^* z_{up}^*$ and $M_c \doteq M_c^{both} = M z_{both}^*$. The core becomes extensive (order N) above the critical value $\gamma_c^{both} = k^{-1}$ (Fig. 5.c).

The analytical approach described so far evaluates the mean value of the number of nodes in the core, in the thermodynamic limit $N \rightarrow \infty$. In order to access the fluctuations around this value we use direct simulation. The shape of the distributions changes significantly with varying γ and number of elements. Figure 6.a shows the distributions of M_c with varying γ . Below the critical value, M_c is condensed around zero, i.e. the graphs are typically close to being tree-like. Near the transition, the distributions have broad tails, and for $\gamma \gg \gamma_c$ they become symmetric around the value found with mean-field LR equations. This phenomenology is typical of phase transitions. In brief, the results show the presence of a phase transition, with varying the order parameter γ , between a region of typically tree-like graphs and a region of extensive feedback loops. These conclusions hold independently from the in-degree value k . Figure 6.c shows the consequence of finite sizes on the LRb algorithm on the transition: the peak of the variance plot indicating the transition point is shifted to greater values and, increasing the system dimensions, it slowly approaches the value k^{-1} . Even for systems with more than 10^4 nodes, the critical point does not reach the analytically determined value. We call γ_e the maximum of the variance of M_c i.e. the effective critical value of γ at finite system size ($\gamma_e \rightarrow \gamma_c, N \rightarrow \infty$). In the region $\gamma_c \leq \gamma \leq \gamma_e$, a residual LRb core is observed and, as we will see, this affects the dynamics. Thus, for small networks, γ_e does not distinctly separate the region characterized by tree-like graphs and the one defined by feedback regions which are present also before this value. This can be also observed in Fig. 6.b which presents the scaling of M_c/N . At a value of $\gamma = 0.35$, M_c may seem to be a sub-extensive quantity. However, increasing N it appears clear that the core is extensive, as the LR equations predict. Taking simulations of very large systems (up to $5 \cdot 10^5$ nodes), values of the fraction of remaining nodes in the core are comparable with which ones obtained from the analytic calculation.

D. Feedback structure at the transition

Let us now take a closer look at what happens around the critical point of LR algorithms. Figure 5.d shows that the three variants of LR have a different trend just after the transition value. Defining $\epsilon = \gamma - \gamma_c$, for small $\epsilon > 0$ the rescaled times of arrest z (i.e. the solutions of the equations $f_0(z_{up}^*) = 0$ and $p_0(z_{down}^*) = 0$, see Appendix A) become

$$\begin{aligned} z_{up}^* &\simeq 2k\epsilon(1 - 2k\epsilon) \simeq 2k\epsilon \\ z_{down}^* &\simeq \frac{2\epsilon k^2}{k-1}(1 - 2\epsilon k) \simeq \frac{2\epsilon k^2}{k-1} \end{aligned}$$

and for LRb:

$$z_{both}^* = z_{up}^* z_{down}^* \simeq \frac{4k^3}{k-1} \epsilon^2 = \frac{4k^3}{k-1} (\gamma - \gamma_c)^2.$$

These functions are continuous at the transition but not all their derivatives are. The discontinuity in z_{both}^* is of greater order than the others, signature of transitions of different orders.

We will now consider the topology of networks with $\gamma \simeq \gamma_c$ (critical networks). Starting from Eqns. (5) we can write

$$f_1 = \frac{1}{z_{up}^*} e^{-\lambda(z_{up}^*)} \lambda(z_{up}^*) \simeq e^{-2k\epsilon} \simeq 1 - 2k\epsilon + O(\epsilon^2)$$

$$p_1 \simeq \left(1 - \frac{2k\epsilon}{k-1}\right)^{k-1} \simeq 1 - 2k\epsilon + O(\epsilon^2),$$

concluding that $\frac{f_2}{f_1} \sim \epsilon$ and $\frac{p_2}{p_1} \sim \epsilon$. This means that, near to the transition point and at the thermodynamic limit, core matrices typically have one entry only per-column *and* per-row. In other words, they are permutations of the identity matrix (and consequently they are invertible). Thus, we can think of the residual (LRb) core as a particular Kauffman network with in-degree one [15, 34]. There is, however, an important difference. In Kauffman networks with in-connectivity one, a node can have more than one outgoing edge, while in this case all nodes in the core must regulate exactly one element; there are no nodes without output (otherwise they would have been removed by the algorithm).

Having one entry per column and per row, core matrices correspond to graphs in which all nodes have (typically) one input and one output, and they show a structure with simple loops disconnected from each other (Figs. 7.b and 7.c). Simulations suggest the presence of several disconnected components that increase in number when the dimension N of the system increases. With growing N , the number of tree-like graphs, as well as the number of cores with only one connected component, decreases (Fig. 6.d). The organization in disconnected loops does not depend on the in-connectivity degree k . The number of nodes in the core of critical networks scales as N^ζ with $\zeta \simeq 0.4$ (Appendix B).

E. Connecting feedback topology and dynamics: reduced dynamics

Since topology and XOR dynamics are strictly related, one would expect that the feedback topology transitions have a repercussion on the evolution of states. We first observe that, around the transition point, the matrices are invertible, hence $d = 0$ (Section III A). From this, the probability of having at least one fixed points falls down at the transition. On the other hand, before the transition one expects to have only fixed points, because of the tree-like structure of graphs. We can rearrange the indices of the matrix S and place *leaf* variables (erased

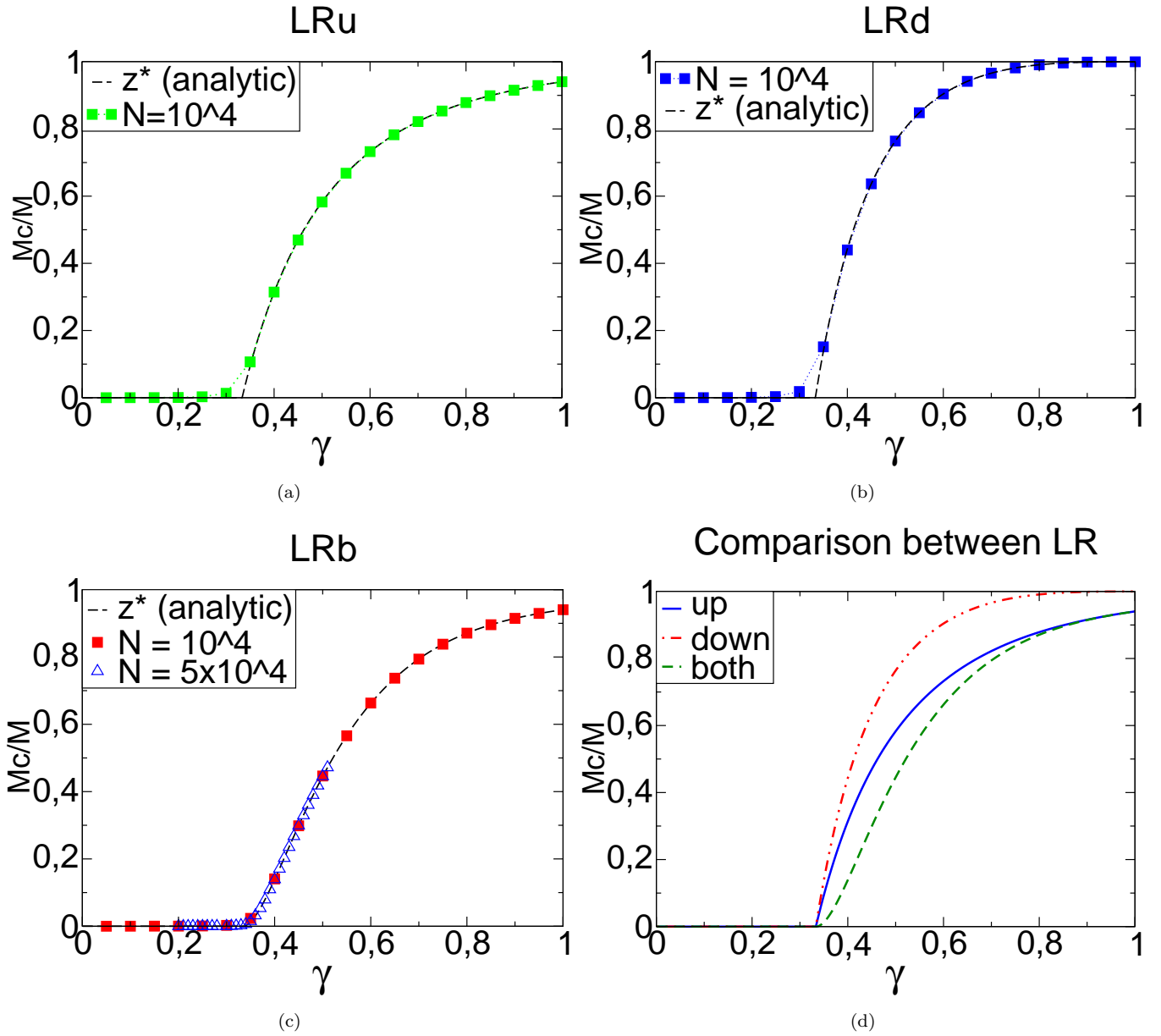


FIG. 5: **Phase transition for LR algorithms** ($k = 3$). The dashed lines represent the fraction of nodes removed by LR up (a), LR down (b) and LR both (c) calculated for different values of γ . Squares are numerical results for graphs with $N = 10^4$ nodes and blue triangles in (c) are the simulations for $N = 5 \cdot 10^4$. Each point is obtained averaging 10^4 simulations. Error bars are smaller than the dimension of the points. The discontinuity of the derivative points to the emergence of an extensive feedback core at $\gamma = \frac{1}{3}$. (d) Comparison of analytic curves for the three variants of the algorithm.

by LRu) in the first indices and *roots* (erased by LRd) in the lasts. In this way it takes the form [26]:

$$S = \left(\begin{array}{c|c} \mathcal{L} & \\ \hline 0 & \mathcal{C} \\ \hline 0 & \mathcal{R} \end{array} \right).$$

Nodes belonging to the LRb core are collected in the sub-matrix \mathcal{C} which has Mz_{both}^* rows. Applying S to a vector

of the form $\vec{x}(t) = (\vec{l}(t), \vec{c}(t), \vec{r}(t))$ (see Eq. (2)) one concludes that the evolved state of roots, $\vec{r}(t)$, is fixed only by initial conditions and remains constant. The nodes \vec{c} belonging to the LRb core are determined by both \vec{r} and \vec{c} itself. Finally, the configuration of leaf nodes \vec{l} is established by all the variables and is not affected by feedback. Thus, the behaviour of the whole dynamics can be deduced from the state of the core. For these reasons, simulations of the dynamics restricted to the core (*reduced dynamics*) are sufficient to evince the

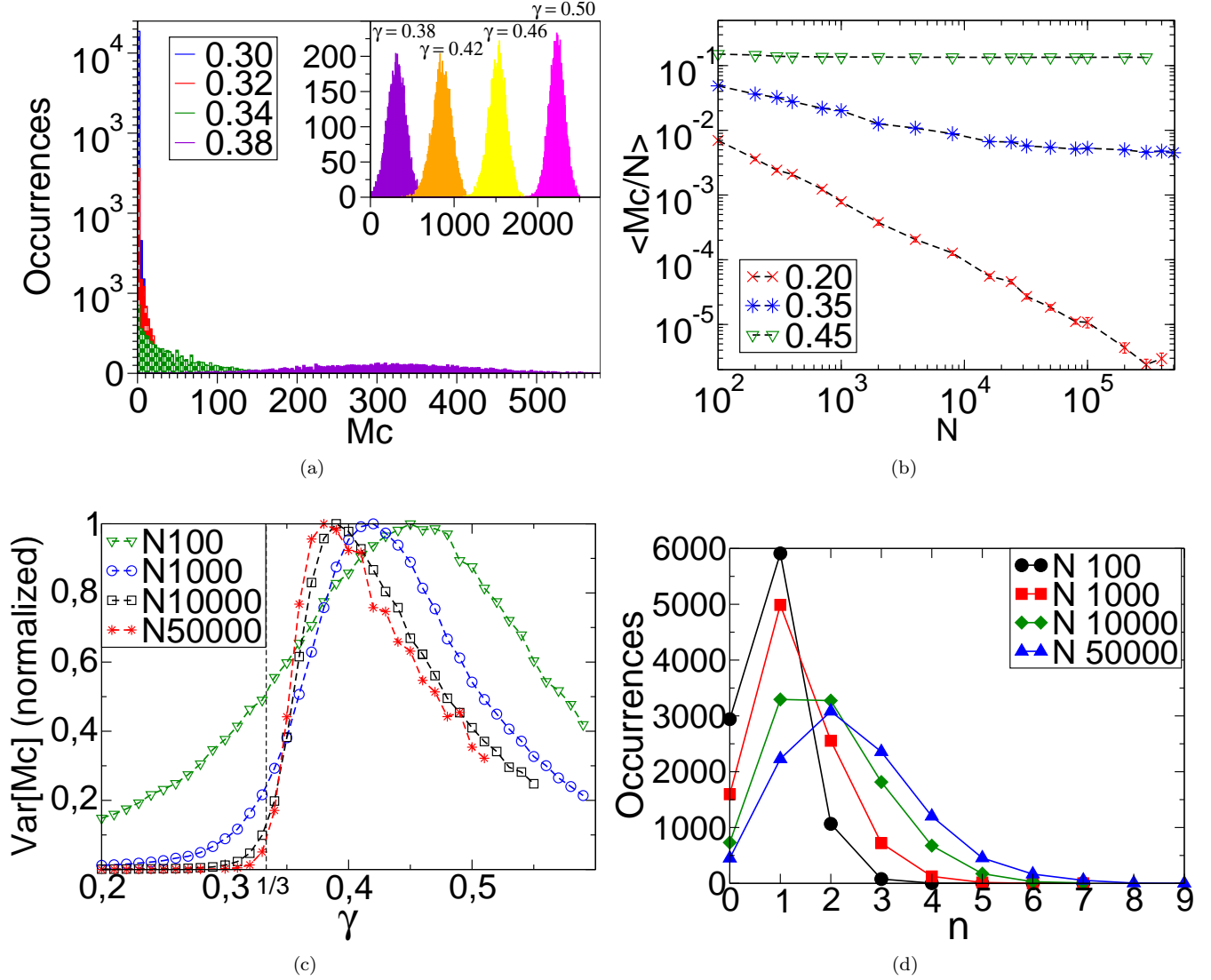


FIG. 6: **Feedback core.** (a) Histograms of core size M_c obtained from simulation of LRb for $k = 3$, $N = 10^4$ and 10^4 different networks (colors online). The inset reproduces the same plot for values of γ equal to 0.38, 0.42, 0.46 and 0.50. (b) Fraction of nodes in the LRb core. Points represent the averaged values resulting from simulations (ensembles composed by 10^4 networks or 10^3 for large systems) for different values of γ : 0.20 (red online), 0.35 (blue online) and 0.45 (green online). (c) Variance of the fraction of the number of nodes belonging to the core at varying N . For fixed values of N the number of connected parts does not remarkably change remaining around the critical value of γ (right). 10^4 iterations for each value of N are simulated.

salient features of the dynamics. Using this fact, we are able to simulate networks with up to 10^3 nodes with a large statistic. On the other hand, obtaining data in the chaotic region is very difficult also using the reduced dynamics (see Fig. 8).

Nevertheless, the region immediately after γ_c is interesting, because it carries the consequences of the simplified core structure in the topology. The equations for critical core variables are special cases of Eq. (1) when each node i receives one input from node $j(i)$:

$$c_i(t+1) = c_{j(i)}(t) + b_i ,$$

In case the core is a single component, then the maximum period length T_{max} will be approximately equal to M_c . Since, near the transition, core matrices are invertible Eq. (3) becomes $S_c^{t_m} = 1$ ($l = 0$). The condition to have the maximum period is

$$\vec{c}(T_{max}) = S_c^{T_{max}} \vec{c}(0) + \Sigma(T_{max}) \vec{b} = \vec{c}(0) .$$

The matrices S_c are also permutation matrices with dimension $M_c \times M_c$ and thus $S_c^{M_c} = 1$. Since $\Sigma(2M_c) = 0$, the maximum period achievable is $T_{max} = 2M_c \sim M_c$. In case the core is formed by several disconnected chains, the maximum period of the whole network can be computed as the least common multiple of the period of each single loop.

More in detail, we estimate T_{max} considering cores built of *loop* structures [44] of lengths the first m prime numbers $\{p_1, p_2, \dots, p_m\}$, so:

$$M_c = \sum_{i \leq m} p_i , \quad T = T_{max} = \prod_{i \leq m} p_i .$$

Since the n th prime number scales as $n \ln n$, from the above equations one has

$$M_c \sim \sum_n^m n \ln n \sim \frac{1}{2} m^2 \ln m$$

$$\ln T_{max} \sim \sum_n^m \ln n + \ln \ln n \sim m \ln m ,$$

from which

$$\ln T_{max} \sim \sqrt{M_c \ln M_c} . \quad (6)$$

Simulated graphs show that this expression is a good upper bound for the value of $T = \text{LCM}\{l_i\}$ (Fig. 9.a). The plots indicate that these values “thicken” around multiple values of M_c . This suggests that residual graphs have a large component with dimension roughly equal to M_c and a short loop of length 2, 3, ...

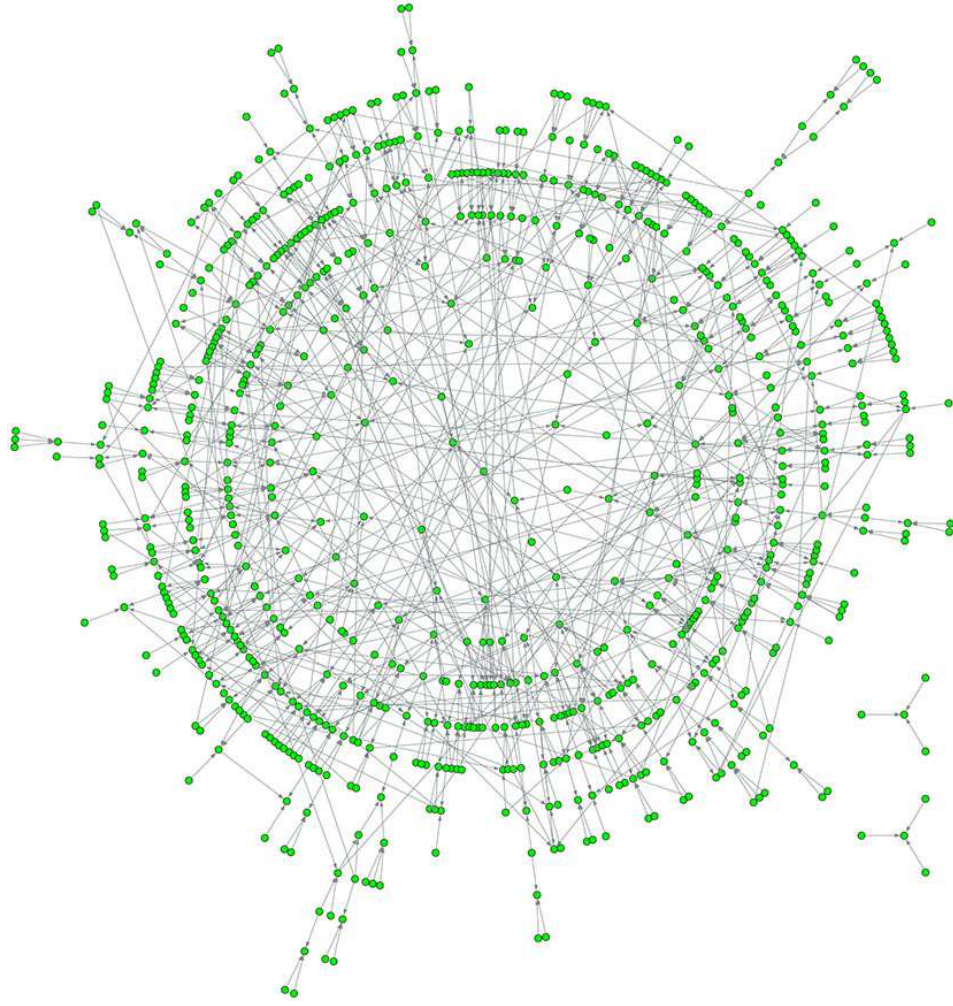
It is interesting to compare these estimates with maximum-length cycles generated by simulations of the core dynamics. Our numerical plots show the values of the maximum period T_{max} emerging from reduced dynamics. In the case $N = 99$ the bound set by

Eq. (6) is passed several times (Fig. 9.b) because of finite size effects, but it becomes more reliable for larger systems. Figure 9.c shows that simulated values for T_{max} seem to concentrate under the function $g(M_c) \sim \exp(\sqrt{M_c \ln M_c})$. Finally, Fig. 9.d shows the maximum cycle distributions for the same simulations. These are power-law like, and become broader with the system dimension. Since statistics is limited by the imposed cutoff, averages are highly biased by this computational restriction and cannot be considered reliable for large systems or much beyond the critical line.

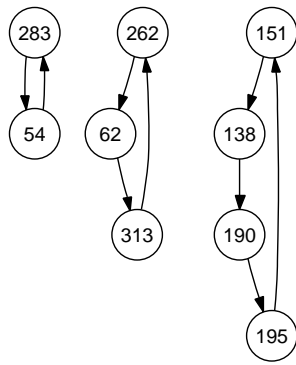
IV. DISCUSSION AND CONCLUSIONS

In this work, we considered a model of Random Boolean Networks related to Kauffman networks. The model has the objective to investigate on abstract grounds some features that are important in biological networks, mainly (1) the presence of nodes which regulate but are not regulated, existing in empirical transcription networks, and (2) the correspondence between topology and dynamics. For the latter reason we chose to use a XOR dynamics to define the interaction between elements. We have shown that in this model the dynamical aspects characterizing the length of cycles and their basins of attraction are direct consequences of the topological feedback structure of the underlying networks, which we study with graph decimation algorithms (LRs) on a fixed in-degree ensemble of graphs.

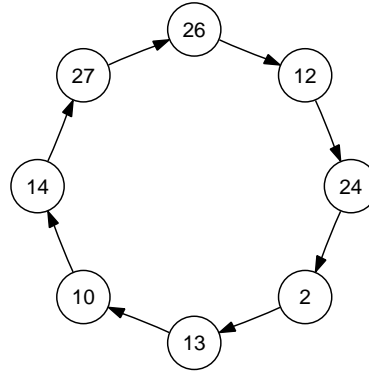
We identified a dynamical and topological phase transition with varying input structure of the graphs modulated by the parameter γ (the fraction of the input-receiving nodes). Direct numerical simulations of the dynamics (Figs. 2 and 3) suggest the presence of a phase transition where long cycles emerge. Correspondingly, a topological phase transition separates a tree-like graph region from one in which extensive feedback components are present. Different Leaf Removal algorithms that remove the upstream tree-like regions, the downstream ones, or both, have the same critical point $\gamma_c = k^{-1}$, which we locate analytically and numerically. The dynamic transition is found numerically at a critical value that is close to γ_c , but strongly influenced by finite size effects. Since networks below the transition typically exhibit fixed points, and this behaviour is correlated with the tree-like structure of these graphs, we identify the dynamic transition point with γ_c in the thermodynamic limit. Thus, despite of the large finite-size effects which make the simulations difficult, our results lead to the conclusion that the topological and dynamic transitions are the same. Above the transition (Fig. 3) the presence of an extensive feedback region induces chaotic dynamics, characterized by exponential cycles (order 2^{M_c} with $M_c \sim O(N)$). In this case, the initial conditions, and thus the influence of the external world, do not affect the dynamics. For this reason, studying the features of networks away from the transition is only relatively in-



(a)



(b)



(c)

FIG. 7: **Structure of a critical core.** (a) shows a realization of a simulated network with $N = 10^3$ and $M = 333$ (potential isolated nodes are not depicted). It can be noticed that each regulated node receives exactly $k = 3$ inputs. The structure is highly simplified after the application of LRb: only three disjoint simple loops are present (b). Panel (c) reports another typical chain structure of a core made of a single connected component (the starting graph had $N = 100$ and $M = 33$).

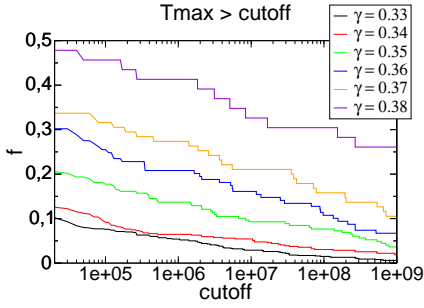


FIG. 8: Fraction f of networks which have a T_{max} greater than a cutoff. Simulations made for networks with $N = 999$ and $k = 3$. From $\gamma = 0.33$ to $\gamma = 0.38$ we respectively simulated 1000, 589, 284, 149, 95, 46 different realizations of the model.

teresting.

The most interesting region to study is the transition point, where the dynamics can be at the same time non-trivial and under external control. At this point, our analytical mean field theory predicts that the structure of feedback components in the graph is simple. Feedback components (independently from the in-degree) show an elementary modular organization in simple disconnected loops, found in simulations (Fig. 7) and predicted by the analytical approach. In turn, this feedback structure transposes to a modular dynamics, which can be completely characterized by the LCM structure of periods. We give an analytical (large N) prediction for the maximum cycle achievable. Comparing with (small N) simulations (Fig. 9), the distribution of the maximum cycles is wide but, with increasing dimension of the system, the estimate becomes increasingly reliable and comparable with the prediction. This point might have an interest for the modeling of empirical biological networks (which have N of the order of a few thousand). Indeed, at these “realistic” system sizes, this point corresponds to an interval with a finite span, because of finite-size effects, as it happens with Kauffman networks [35].

It is interesting to make a comparison between the model used here and Kauffman networks. In the latter model, the dynamics is entirely controlled by so-called relevant nodes [34, 36] which have been the subject of many studies [35, 37, 38, 39]. In networks between the chaotic and the stable phase, they spontaneously organize into disconnected clusters whose number increases logarithmically with the system size [37, 40]. Most of relevant clusters are simple loops. The number of relevant nodes in critical networks scales as $N^{1/3}$ in the limit $N \rightarrow \infty$ [35]. As recently found by Drossel and coworkers [37, 41, 42], since the relevant part constitutes only a vanishing portion of the network, the topology of Kauffman networks is most likely very different from the topology of real biological networks, such as genetic regulatory networks, where one would expect that the majority of nodes is relevant or at least not always frozen. We can carry the analogy between relevant components

of Kauffman networks and the LRb core of the γ model in critical networks. The core is in fact the only part of the whole graph responsible of the dynamic behaviour as relevant nodes are in Kauffman networks. We find that the critical core has a modular structure and the amount of disconnected loops increases as the system size grows. With our model, it is possible to explain analytically this ordered organization in the mean-field limit. Simulations show that the number M_c of nodes belonging to the core scales as N^ζ with $\zeta \simeq 0.4$.

In conclusion, the γ model, considering the whole graph as a regulatory network, gives a basic phenomenology that could be exploited in constructing a prototypic model of genetic regulation networks, introducing for example more realistic graph ensembles [43] and representations for the input functions.

APPENDIX A: LEAF REMOVAL EQUATIONS

1. Leaf Removal up

To write the mean-field equations for this algorithm, we analyze the evolution of connectivities of the regulated nodes only, which are specified by the matrix S . The number of LR steps is the time t of the process and is the number of nodes that have been removed. We introduce the *normalized time* $\bar{t} = t/M$, $\bar{t} \in [0, 1]$ so that $\Delta \bar{t} = M^{-1}$ and $\Delta c_n = M \Delta f_n = \frac{\partial f_n}{\partial \bar{t}}$.

At time $t = 0$, the probabilities f_n (see Section III C) are

$$\begin{cases} f_X(0) = 0 \\ f_n(0) = e^{-\gamma k \frac{(\gamma k)^n}{n!}} \doteq e^{-\lambda(0) \frac{\lambda(0)^n}{n!}}, \quad n \geq 0, \end{cases} \quad (\text{A1})$$

f_X indicating the fraction of erased nodes. When $M f_X(\bar{t}) = M \bar{t}$ nodes are removed, $c_n(\bar{t}) = M f_n(\bar{t})$ nodes with n outgoing edges remain. When a node without outgoing edges is found, it is removed (it corresponds to a column of the matrix with no elements different from 0) so that at each step $M f_X$ increases of one unit. Also its incoming links are removed, which means that the corresponding row in S is cleared out, replacing with zero all the entries. Removing edges changes the probability distribution $f_n(\bar{t})$. Indeed the probability that an edge that is being removed comes from a node with n outgoing edges (this one becoming an $n - 1$ outgoing edges node) is

$$P_{[n \rightarrow n-1]} = \frac{n c_n(\bar{t})}{\sum_{n \geq 1} n c_n(\bar{t})} = \frac{n f_n(\bar{t})}{\sum_{n \geq 1} n f_n(\bar{t})}.$$

so that removing an edge implies $\Delta c_n = -1 \cdot P_{[n \rightarrow n-1]} + 1 \cdot P_{[n+1 \rightarrow n]}$.

Recognizing that we remove, on average, γk edges per step [45], we write the flow equations for the probabilities

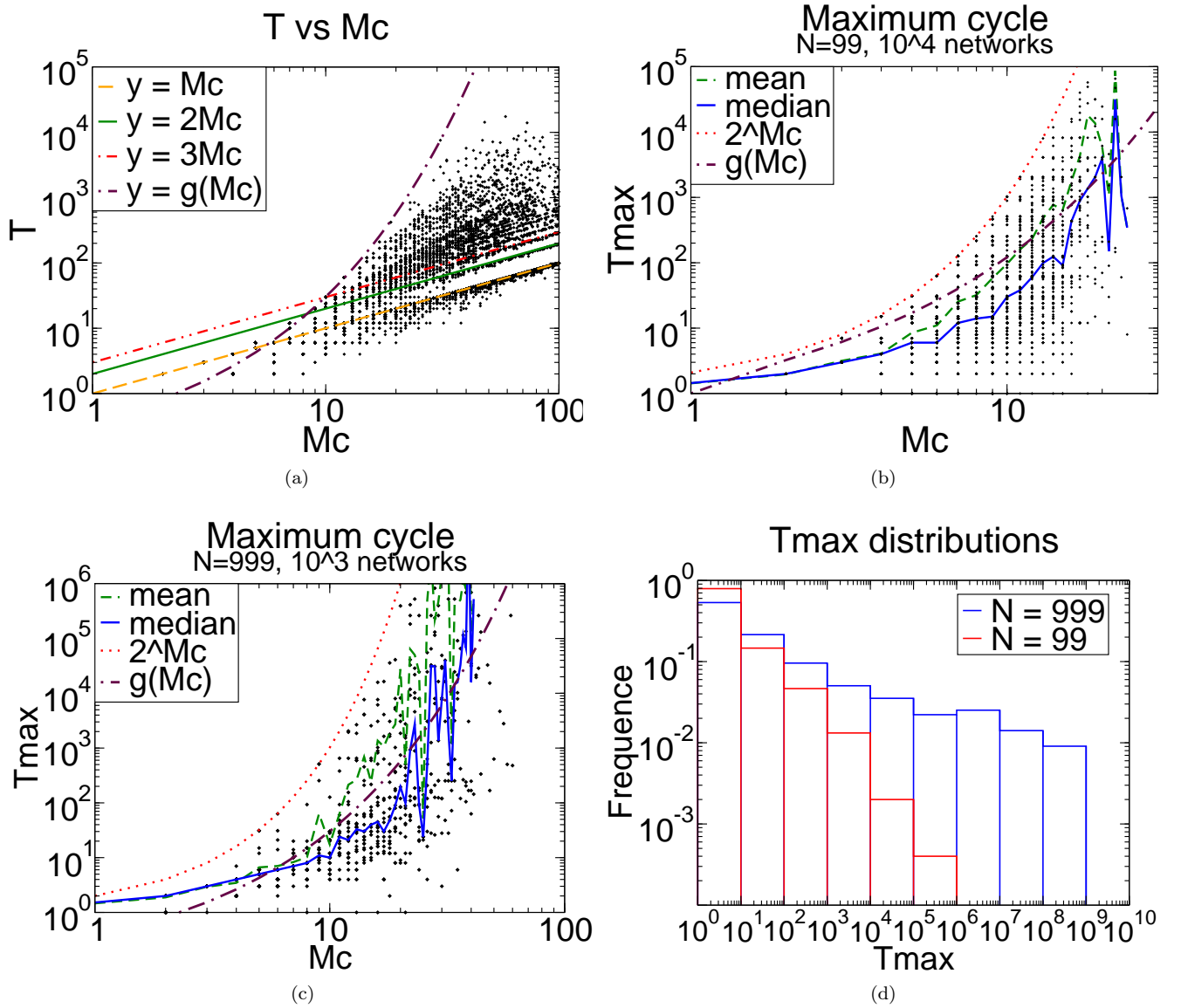


FIG. 9: **Maximum cycle length for critical networks.** (a) Values of $T = \text{lcm}\{l_i\}$ vs Mc for $\gamma = 0.3334$, $N = 10^4$, and 10^4 different networks. $g(Mc) \sim \exp(\sqrt{Mc \ln Mc})$. (b) and (c) are numerical simulation of the dynamics of core networks at $\gamma = 0.33$ ($k = 3$). The plots report the values of T_{max} as a function of Mc . Dots are experimental points compared with the bound $g(Mc) \sim \exp(\sqrt{Mc \ln Mc})$. Solid line (blue online) reports the median and the dashed one (green online) the mean. The cutoff on cycle lengths is 10^9 . For $N = 999$ (c) this limit is passed only six times and all for $Mc \geq 48$. Estimates of central values are not calculated when data are insufficient. (d) Shape of the distributions of T_{max} for $N = 99$ (red online) and $N = 999$ (blue online). The distributions are power-law-like and their tails are limited by the cutoff imposed (10^9).

$f_n(\bar{t})$ as follows:

$$\begin{cases} \frac{\partial}{\partial \bar{t}} f_X(\bar{t}) = 1 \\ \frac{\partial}{\partial \bar{t}} f_0(\bar{t}) = -1 + \frac{\gamma k}{\langle n \rangle(\bar{t})} f_1(\bar{t}) \\ \vdots \\ \frac{\partial}{\partial \bar{t}} f_n(\bar{t}) = \frac{\gamma k}{\langle n \rangle(\bar{t})} [(n+1)f_{n+1}(\bar{t}) - nf_n(\bar{t})] \end{cases}, \quad n > 0 \quad (\text{A2})$$

with initial conditions (A1) and where $\langle n \rangle(\bar{t}) = \sum_{n \geq 1} n f_n(t) = \sum_{n \geq 0} n f_n(t) = k\gamma(1 - \bar{t})$ being the aver-

age number of edges per node after $M\bar{t}$ remotions. One can easily check that the poissonian $f_n(t)$ given in Section III C are solutions of Eqns. (A2) once having imposed

$$-\frac{d\lambda(\bar{t})}{d\bar{t}} = \frac{\gamma k}{\langle n \rangle(\bar{t})} = \frac{1}{1 - \bar{t}},$$

from which $\lambda(\bar{t}) = \gamma k(1 - \bar{t})$. See Ref. [26] for details. The algorithm stops when $f_0(\bar{t}) = 0$, i.e. at time $\bar{t}^* = e^{-\lambda(\bar{t}^*)}$. This equation implies that if $\gamma k < 1$ the stop

normalized time is $\bar{t}^* = 1$ or, in other words, all the graph is removed. There is a critical value of γ , $\gamma_c = k^{-1}$, below which the whole graph is cancelled after the application of LRu. These networks typically have a tree-like structure without feedback regions.

Being t the number of variables deleted, it is useful to introduce the variable

$$z_{up} \doteq 1 - \bar{t} = 1 - \frac{t}{M} = \frac{M-t}{M}.$$

which expresses the fraction of remained nodes during the LRu process.

2. Leaf Removal down

In the first LRd step, all the $N - M$ unregulated nodes are eliminated from the network because they have no inputs (this corresponds to neglecting the matrix R and working with only the square matrix S).

As above, the time t of the algorithm represents the number of removed nodes. It is again useful to employ a normalized time \bar{t} . The number of nodes with n entries at time t is $r_n(t) = Mp_n(t)$ where $p_n(t)$ is the probability introduced in Section III C. At time $t = 0$ it reads:

$$\begin{cases} p_X(0) = 0 \\ p_n(0) = \binom{k}{n} \gamma^n (1-\gamma)^{k-n}, \quad 0 \leq n \leq k, \end{cases}$$

where p_X is the fraction of removed nodes. In the decimation algorithm a node with no entry is cleared out together with its outgoing connections, so that probability $p_n(t)$ changes. At each step, the number of emptied rows r_X increases by one and we obtain

$$p_X(\bar{t}) = \bar{t} \quad \sum_{i \geq 0} p_i(\bar{t}) = 1 - \bar{t}.$$

The probability that a removed edge was input for a node with n ingoing edges is:

$$P_{(n \rightarrow n-1)} = \frac{nr_n(t)}{\sum_{n \geq 1} nr_n(t)} = \frac{np_n(\bar{t})}{k\gamma(1-\bar{t})}$$

where we remembered that $\langle n \rangle(\bar{t}) = k\gamma(1-\bar{t})$.

Once again, an average number $k\gamma$ of edges are removed at each step so that a node with n entries becomes, with probability $k\gamma \cdot P_{(n \rightarrow n-1)}$, a node with $n-1$ entries. Thus, one can write the flow equations:

$$\begin{cases} \frac{\partial}{\partial z} p_X(z) = -1 \\ \frac{\partial}{\partial z} p_0(\bar{t}) = 1 - \frac{p_1(z)}{z} \\ \vdots \\ \frac{\partial}{\partial z} p_n(z) = n \frac{p_n(z)}{z} - (n+1) \frac{p_{n+1}(z)}{z} \quad n \leq k, \\ p_{k+1} = 0, \end{cases}$$

where we have already made the substitution $z = z_{down} = 1 - \bar{t}$, $z_{down} \in [0, 1]$. In Section III C we give the solutions to these equations. The process ends when no more unregulated nodes are available, that is when $p_0(z) = 0$, namely when $1 - z = (1 - \gamma z)^k$. Studying this condition one sees that if $\gamma < k^{-1}$ then there are no solutions apart from the value $z = 0$, which indicates the existence of a tree-like graph in which all is removed.

APPENDIX B: FINITE SIZE EFFECTS

According to our simulations, finite size effects appear to be very relevant both in topological structure and dynamic behaviour. Increasing N , the shape of the distribution remains the same and it is more peaked around the central value predicted by LR equations.

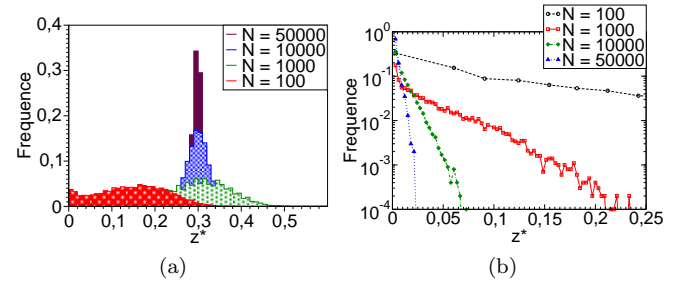


FIG. 10: Distributions of the number of nodes belonging to the LRb core for different system dimension at fixed γ . General case (a) with $\gamma = 0.45$ and critical networks (b). Simulations are produced by 10^3 iterations for $N = 5 \cdot 10^4$ and 10^4 iterations otherwise.

Furthermore, it can be observed that M_c scales with N as a power law with exponent lower than 1 (simulations suggest a trend $M_c \sim N^\zeta$ with $\zeta \simeq 0.4$), while nodes upstream the core that are removed by LRd and nodes downstream removed by LRu grow approximately linearly in N . Figures 11 show the results of simulations. The upstream part of the graph removed by LRd is indicated with the letter U and the downstream part with D . One speculates that U , D and M_c at the transition point behave as

$$U \sim \alpha N \quad D \sim \beta N \quad M_c \sim N^\zeta.$$

Also the particular core structure of critical networks is affected by finite size effects. In fact, for $N = 100$ it is not unusual to find core networks with more complex structures than disconnected simple loops. This also explains the behaviour of Fig. 6(d): one can speculate from the plots that the LRb core description in modular structures becomes more accurate increasing N , while, for smaller systems and $\gamma_c \leq \gamma \leq \gamma_e$, a single disconnected component with a more complex structure is present with more frequency.

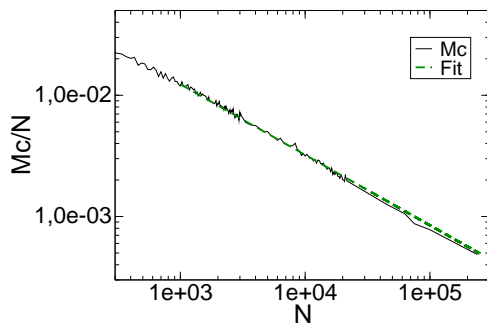


FIG. 11: Scaling with N of the core M_c . Each point of simulation is the averaged result of 10^3 iterations. The fit $y = ax^b$ with $a \simeq 0.68$ and $b \simeq -0.58$ is presented.

-
- [1] A. L. Barabasi and Z. N. Oltvai, *Nat. Rev. Gen.* **5**, 101 (2004).
 - [2] U. Alon, *Science* **301**, 1866 (2003).
 - [3] L. H. Hartwell, J. J. Hopfield, S. Leibler, and A. W. Murray, *Nature* **402**, C47 (1999).
 - [4] D. Bray, *Science* **301**, 1864 (2003).
 - [5] Z. N. Oltvai and A. L. Barabasi, *Science* **298** (2002).
 - [6] T. I. Lee et al., *Science* **298**, 799 (2002).
 - [7] M. Babu, N. Luscombe, L. Aravind, M. Gerstein, and S. Teichmann, *Curr. Opin. Struct. Biol.* **14**, 283 (2004).
 - [8] R. Thomas, *J. Theor. Biol.* **42**, 563 (1973).
 - [9] S. A. Kauffman, *The origins of order : self-organization and selection in evolution* (Oxford University Press, New York, 1993).
 - [10] N. Guelzim, S. Bottani, P. Bourguine, and F. Képès, *Nat. Genet.* **31**, 60 (2002).
 - [11] M. Isalan, C. Lemerle, K. Michalodimitrakakis, C. Horn, P. Beltrao, E. Raineri, M. Garriga-Canut, and L. Serrano, *Nature* **17**, 840 (2008).
 - [12] S. A. Kauffman, *J. Theor. Biol.* **22**, 437 (1969).
 - [13] C. Gershenson, in *Workshop and Tutorial Proceedings, Ninth International Conference on the Simulation and Synthesis of Living Systems (Artificial Life IX)*, edited by M. Bedau, P. Husbands, T. Hutton, S. Kumar, and H. Suzuki (MIT Press, 2004), pp. 160–173.
 - [14] M. Aldana, S. Coppersmith, and L. P. Kadanoff, in *Perspectives and Problems in Nonlinear Science, A celebratory volume in honor of Lawrence Sirovich*, edited by E. Kaplan, J. E. Marsden, and K. R. Sreenivasan (Springer, New York, 2003), Springer Applied Mathematical Science Series, pp. 23–89.
 - [15] B. Drossel, in review to appear in *Annual Review of Nonlinear Dynamics and Complexity*, edited by H. Schuster (Wiley, 2007), vol. 1, URL <http://arxiv.org/abs/0706.3351>.
 - [16] U. Bastolla and G. Parisi, *J. Theor. Biol.* **187**, 117 (1997).
 - [17] A. S. N. Seshasayee, P. Bertone, G. M. Fraser, and N. M. Luscombe, *Curr. Opin. Micr.* **9**, 511 (2006).
 - [18] N. M. Luscombe, *Nature* **431**, 308 (2004).
 - [19] S. Balaji, M. Madan Babu, and L. Aravind, *J. Mol. Biol.* **372**, 1108 (2007).
 - [20] U. Paul, V. Kaufman, and B. Drossel, *Phys. Rev. E* **73**, 026118 (2006).
 - [21] B. Samuelsson and C. Troein, *Phys. Rev. Lett.* **90**, 098701 (2003).
 - [22] B. Drossel, *Phys. Rev. E* **72**, 016110 (2005).
 - [23] M. Cosentino Lagomarsino, P. Jona, and B. Bassetti, *Phys. Rev. Lett.* **95**, 158701 (2005).
 - [24] L. Correale, M. Leone, A. Pagnani, M. Weigt, and R. Zecchina, *J. Stat. Mech.* p. P03002 (2006).
 - [25] L. Correale, M. Leone, A. Pagnani, M. Weigt, and R. Zecchina, *Phys. Rev. Lett.* **96**, 018101 (2006).
 - [26] M. Cosentino Lagomarsino, P. Jona, and B. Bassetti, in *Proceedings of the CMSB conference, Lecture Notes in Bioinformatics* (Springer, 2006).
 - [27] V. F. Kolchin, *Random Graphs* (Cambridge University Press, New York, 1998).
 - [28] S. Caracciolo and A. Sportiello, *J. Phys. A: Math. Gen.* **35**, 7661 (2002).
 - [29] M. Mézard, G. Parisi, and M. Virasoro, *Spin Glass Theory and Beyond*, vol. 9 of *World Scientific Lecture Notes in Physics* (World Scientific Publishing Company, 1987).
 - [30] M. Mézard, F. Ricci-Tersenghi, and R. Zecchina, *J. Stat. Phys.* **111**, 505 (2003).
 - [31] M. Bauer and O. Golinelli, *Eur. Phys. J. B* **24**, 339 (2001).
 - [32] M. Weigt, *Eur. Phys. J. B* **28**, 369 (2002).
 - [33] C. Maffi, *Dynamical properties of Boolean models inspired to transcriptional regulation networks* (Master degree thesis, Università degli studi di Milano, 2005-2006).
 - [34] H. Flyvbjerg and M. Kjaer, *J. Phys. A: Math. Gen.* **21**, 1695 (1988).
 - [35] J. E. S. Socolar and S. A. Kauffman, *Phys. Rev. Lett.* **90**, 068702 (2003).
 - [36] S. Bilke and F. Sjunnesson, *Phys. Rev. E* **65**, 016129 (2001).
 - [37] V. Kaufman and B. Drossel, *New J. Phys.* **8**, (228) (2006).
 - [38] P. Krawitz and I. Shmulevich, *Phys. Rev. E* **76**, 036115 (2007).
 - [39] U. Bastolla and G. Parisi, *Physica D* **115**, 203 (1998).
 - [40] U. Bastolla and G. Parisi, *Physica D* **115**, 219 (1998).
 - [41] V. Kaufman, T. Mihaljev, and B. Drossel, *Phys. Rev. E* **72**, 046124 (2005).
 - [42] T. Mihaljev and B. Drossel, *Phys. Rev. E* **74**, 046101 (2006).

- [43] F. Bassetti, M. Cosentino Lagomarsino, B. Bassetti, and P. Jona, Phys. Rev. E **75**, 056109 (2007).
- [44] we call *loop* the topological chains reserving the term *cycle* to the dynamics
- [45] This is the *in*-connectivity which remains constant as remotion does not affect *in*-distribution p_n . The reverse will be true for LRd